Investigation of thermal oscillation induced by dryout in printed circuit steam generator

Jin Su Kwon[a], Sung Gil Shin[a], Jeong Ik Lee[a,*], Sang Ji Kim[b]
[a]*Department of Nuclear and Quantum Engineering, Korea Advanced Institute of Science and Technology, 373-1 Guseong-dong Yuseong-gu,Daejeon 305-701, Republic of Korea*

[b]*Korea Atomic Energy Research Institute*
150 Dukjin-dong, Yuseong-gu, Daejon 305-353, Republic of Korea

[*]*Corresponding author: jeongiklee@kaist.ac.kr*

1. Introduction

Recently, a compact heat exchanger technology has been considered as a potential candidate for Small Modular Reactors (SMR) steam generator application. A printed circuit steam generators (PCSG) is a kind of printed circuit heat exchanger (PCHE), as shown in Figure 1, designed for the steam generator application. This type of heat exchanger has been studied for the steam generator in SMART, a small-sized integral-type PWR developed at KAERI in Korea [1]. The extraordinary structural rigidity of a PCSG comes from the nature of the manufacturing process. PCSG is fabricated by stacking multiple chemical-etched plates and diffusion bonding together under high temperature and pressure. PCHEs generally have 0.5 to 4 mm semi-circular channel diameter, which can provide a large heat transfer area.

Because of the spatial constraint for installing the steam generator inside the pressure vessel with the reactor (i.e. integral reactor), the SMART development group has introduced a once-through steam generator. Thus, a PCSG experiences various boiling regimes including nucleate boiling, dryout, and film boiling to produce superheated steam. The dryout occurs where the liquid film in contact with the heated wall disappears and enters the film boiling region. The movement of dryout front, which is unstable regardless of density wave oscillation, induces a transition in boiling regimes between nucleate boiling and film boiling regimes [2]. It results in a significant wall temperature oscillation that can cause thermal fatigue. This will impact on the component lifetime due to cyclic thermal stresses. Therefore, thermal oscillations induced by dryout have to be studied to estimate the component integrity and service lifetime.

This type of oscillation was studied in a shell and tube steam generators in the past [3, 4]. Most previous studies have been conducted on typical tubing having diameter of 0.5 inch and researches on micro tubes are very limited. Hence, the frequency of wall temperature oscillation at the dryout front in the semi-circular micro channel should be studied through experiments. This paper presents a successive work of the author's previous study [5]. The purpose of this research is to design an experimental facility including a test section in order to investigate the major parameters of thermal oscillation.

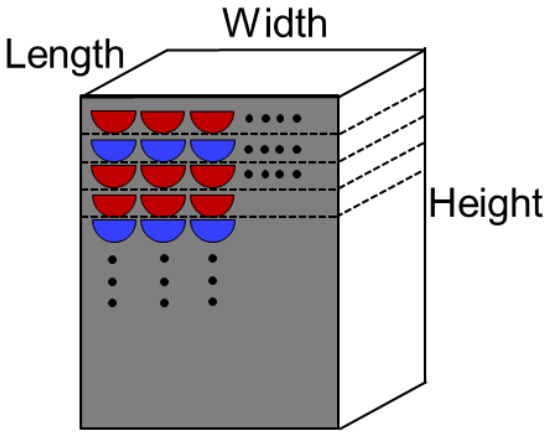

Figure 1. Schematic diagram of the PCHE block

2. Setup for the thermal oscillation experiments

2.1 Main loop

Figure 2 shows the schematic diagram of the experimental facility for the thermal oscillation induced by dryout. The key target of the experimental facility design is matching the aforementioned PCSG operating conditions with the experimental parameters such as heat flux and mass flux at the test section. Deionized water is used for the working fluid as a simulant of the pressurized water side. The facility is a flow loop made up of the test section with the heater, inventory tank, cooler, and pump. The heat into the system is supplied from the preheater and rectifier, respectively. Rectifier, which converts 220 V alternating current into direct current, can transmit the direct current up to 3000 A with voltage up to 10 V to the test section. An immersion heater is used for preheater to maintain the inlet conditions of the test section. With two means of heat source, the water becomes superheated steam inside the test section while experiencing the nucleate boiling, dryout, and post-dryout heat transfer. For the experimental conditions, inlet and outlet temperatures of the test section are fixed to 90 and 110 ^{o}C, respectively. The operating pressure is atmospheric pressure. The superheated steam passing through the test section merges with the water in the bypass line and it is condensed back to water and flows into the inventory tank. In order to prevent the occurrence of two-phase flow instability caused by the rapid volume expansion, a throttle valve is placed at the inlet of the test section.

Moreover, the loop is an open system that is connected to air in the inventory tank to eliminate the system pressure fluctuation. Two bypass lines, which are placed at the outlet of the pump and inlet of the test section, are installed to have better controllability of mass flow rate. The flow loop is constructed with 0.5 inch tube with stainless steel 316 except for test section. The working fluid heated in the heater section is cooled by water at room temperature in the cooler. The loop is designed to operate at pressure up to 5 bar and temperature up to 130 ^{o}C.

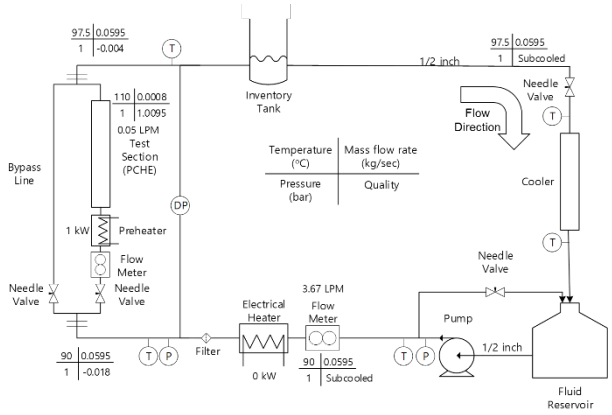

Figure 2. Schematic diagram of the experimental facility

2.2 Test section

As shown in Figure 3, the test section consists of three parts: (1) resistance heating section, (2) visualization window and (3) clamp. To facilitate the sophisticated measurement of experimental parameters, the test section has only one semi-circular flow channel in the middle. To produce the superheated steam in the flow channel, the rectifier supplies the DC current to the resistance heating section. The dimension of the heating section is determined by considering the electrical resistivity and structural stability. When the cross-section is wide, electrical resistivity is decreased, and thus, the current is increased under the same electrical potential difference, which leads to a high heat generation by the Joule's law. On the other hand, the heat loss can be larger due to larger heat transfer area and fixing between resistance heating section and visualization window becomes difficult. The height is fixed to 1 m due to the test section buckling. The semi-circular shaped flow channel and diameter of 2 mm are derived from the optimized PCSG geometry. One difference in the test section from the typical PCSG flow channel is that the 0.5 mm capillary stainless steel tube is inserted at the edge of flow channel. It protects the optical fiber sensor from the boiling of the working fluid and makes it possible to measure the wall temperature stably without the interference of nucleated bubbles. The detailed description of optical fiber sensor will be discussed in the next section. The graphite seals are installed symmetrically with respect to the flow channel between the heating section and visualization window since leakage can cause significant measurement error of the mass flow rate. With the purpose of the visual observation of dryout instability, the visualization window with quartz having a thickness of 5 mm is attached to the heating section. After the experiments, the visual observations of the hydraulic phenomena will be used to validate the measurement of thermal oscillation frequency. The resistance heating section and visualization window are physically bonded by the customized clamp with graphite. The electric resistivity of graphite is about 8 times higher than that of nichrome so most of the direct current flows into the nichrome section. It indicates that Joule heating mainly occurs at the resistance heating section, not the clamp. The reason why the rubber or Teflon is not used at the connections is due to the wall temperature that can be increased up to 550 ^{o}C when dryout occurs in the flow channel. Such a high temperature environment can cause deformation of rubber-like materials so that graphite is chosen as the clamp material.

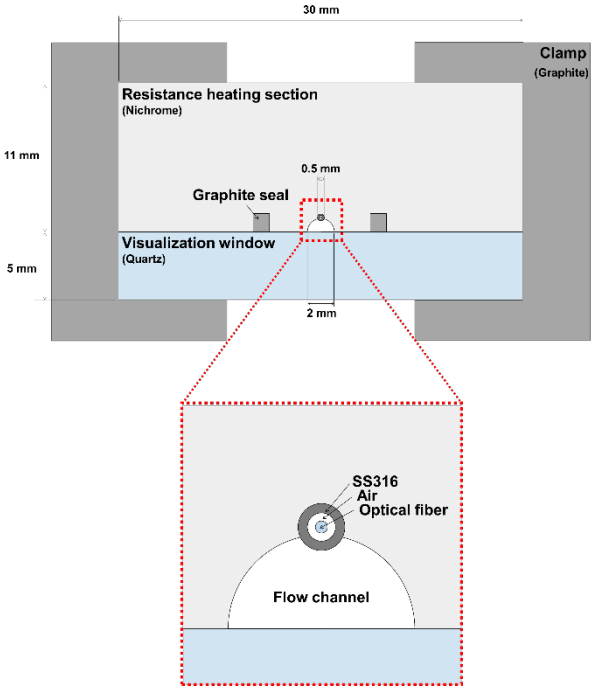

Figure 3. Cross section of the test section

2.3 Optical fiber

The period of the thermal oscillation induced by dryout can be obtained by measuring the wall temperature oscillation near the dryout front. In the previous researches, wall temperature was measured using thermocouples by placing them very densely. For instance, thermocouples are spaced 5 mm apart in the flow direction at the expected dryout occurrence point [6]. Such a traditional method limits experimental conditions due to a fixed place where dryout occurs. In addition, the uncertainty of frequency measurements can be increased with the difficulty in predicting the location of dryout occurrence. In order to resolve the abovementioned problems, a novel concept of temperature measurement system is introduced. The

fiber optic sensing system can acquire the distributed temperature along a single strand of thin optical fiber, which is called a distributed temperature sensor (DTS) [7]. The sensing principle is based on Rayleigh scattering caused by impurities and structural inhomogeneity at the molecular level [7]. Backscattered light is used for analysis to interrogate the status of the fiber. The random distribution of impurities along the fiber core makes an individual backscatter pattern. The wavelength and amplitude of this pattern can be considered as a characteristic of fiber status. This characteristic is altered by the physical changes of fiber such as strain or temperature. Therefore, detecting this characteristic can lead the optical fiber system to be used as a sensor.

A sensing system is made up of a fiber, tunable laser source, and interrogator. The locations of the scattering centers can be obtained by the beat frequencies between the backscattered signal and a reference signal using Fourier transform in the swept wavelength interrogator. Firstly, the baseline of the spectrum is recorded in the reference condition. Then, backscatter amplitude as a function of wavelength is used for calculating the spectrum shift with the baseline signal since the temperature change produces the shift. The spatial resolution for the temperature measurement is typically about 5.12 mm at data acquisition rates up to 50 Hz [8]. Spectrum shifts have a linear relationship with the strain and temperature difference as shown in Equation (1).

$$\frac{\Delta\lambda}{\lambda} = K_T \Delta T + K_\varepsilon \varepsilon \quad (1)$$

K_T and K_ε indicate the temperature and strain coefficients, respectively. The temperature coefficient including the thermal expansion coefficient and the index of refraction has to be fixed in the fiber to be used as a temperature sensor. When acquiring the absolute temperature using the DTS, other temperature measurement devices such as resistance temperature detector and thermocouple are required to establish the absolute temperature for the reference condition. This is because the optical fiber system can only obtain the difference with the reference.

As shown in Figure 3, the optical fiber is placed in the 0.5 mm capillary stainless steel tube to make the fiber remain free of strain as well as noise. Figure 4 shows the picture of optical fiber and the cross section of fiber. Among the various type of fiber coating materials such as polyimide, gold, and copper, the gold coating is used in this study since gold can withstand the high temperature condition up to 700 °C. It is noted that the wall temperature of test section can be up to 550 °C after occurring the dryout due to the deterioration of wall heat transfer. Air is charged in the gap between the optical fiber and stainless steel tube while preventing the fiber from vibration due to the flow of working fluid.

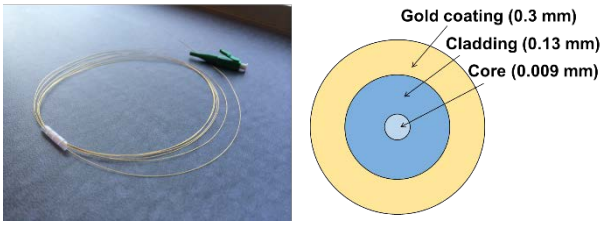

Figure 4. Picture of the gold coating fiber and cross section

2.4 Test section analysis

A preliminary thermal hydraulic analysis of the test section is performed so as to confirm the test section design with a similar analysis method used in the steam generator design scheme. The difference is that the heat transfer rate in the segmental volume is determined by the electrical resistance heating. At first, the constant electrical resistance and current are given for every segmental volume, and then, 1-D FDM analysis proceeds sequentially from the inlet to the outlet. Since the electrical resistivity changes according to the temperature, an iterative process must be followed until the results converge.

Figures 5, 6, and 7 show the temperature distribution of wall and bulk along the axial distance at 2, 3, and 4 mm semi-circular diameter flow channels, respectively. The inlet and outlet temperatures are given at 90 and 110 °C. The wall temperature distributions definitely show the occurrence of dryout near height of 0.8 ~ 0.9 m. The temperature jump after occurring the dryout is very significant compared to that of the PCSG design for SMART. This is because the DC supplier provides the same heat flux along the axial distance on the test section. Heat transfer capability of working fluid is considerably decreased at the downstream of dryout point due to the deficiency of the liquid film. Thus, to sustain the given heat flux condition, a large temperature difference at the dryout point appears. The maximum wall temperature is set to be not larger than 550 °C considering the mechanical properties of stainless steel. It is noteworthy that axial heat conduction is not considered in this analysis to design the test section conservatively. In case the flow channel diameter is 2 mm, the experimental conditions such as heat flux and mass flux are well matched with the operating conditions of the PCSG for SMART. In case the flow channel diameter is 3 and 4 mm, the increased flow area reduces the Reynolds number, which in turn lowers the heat transfer coefficient. It results in fairly decreased mass flux and heat flux for wall temperature constraints, which are not useful operating regions for practical engineering. To address the abovementioned issue, an immersion type heater with 1 kW capacity is used for preheater which is installed at the inlet of the test section. By providing the heat before entering the test section, the heat flux inside the test section becomes decreased so that the mass flux can be increased while meeting wall temperature constraints. The analysis results are summarized in Table I.

Generally, when using common metal alloys such as stainless steel, the specific electrical resistivity is proportional to the temperature. Thus, the designed test section can cause local heat flux to be greater near the dryout point due to the rapid temperature rise if the stainless steel is used. Figure 8 shows the temperature distribution in the stainless steel test section under the same mass flux condition with the nichrome. Figure 9 shows the electrical resistance distributions of both cases. Therefore, the resistance heating section is fabricated with nichrome to give the near constant heat flux conditions along the flow direction.

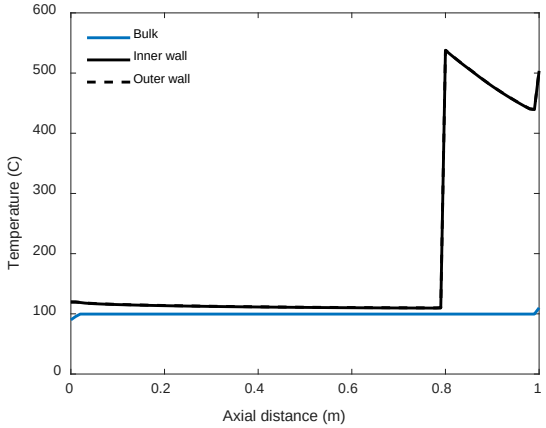

Figure 5. Temperature distribution along the axial distance (2 mm of semi-circular diameter)

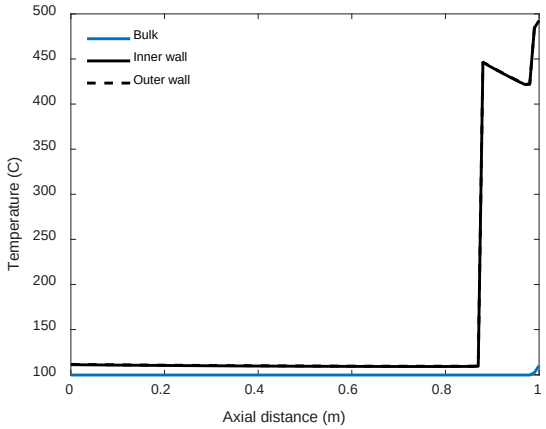

Figure 6. Temperature distribution along the axial distance (3 mm of semi-circular diameter)

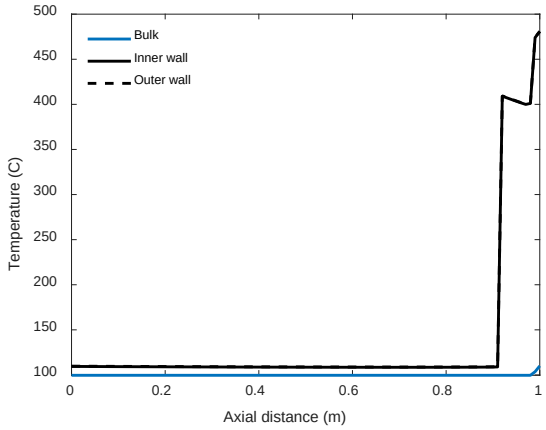

Figure 7. Temperature distribution along the axial distance (4 mm of semi-circular diameter)

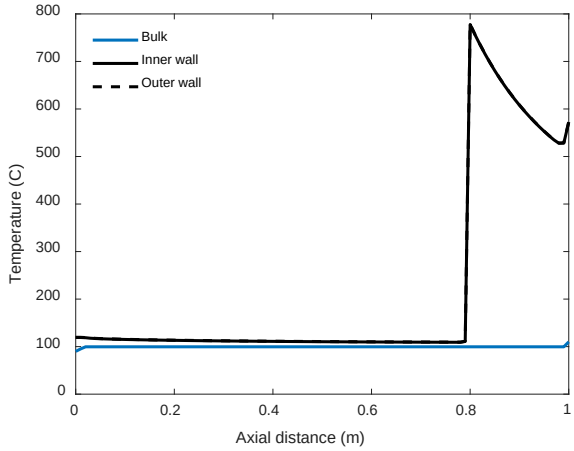

Figure 8. Temperature distribution along the axial distance (2 mm of semi-circular diameter with stainless steel)

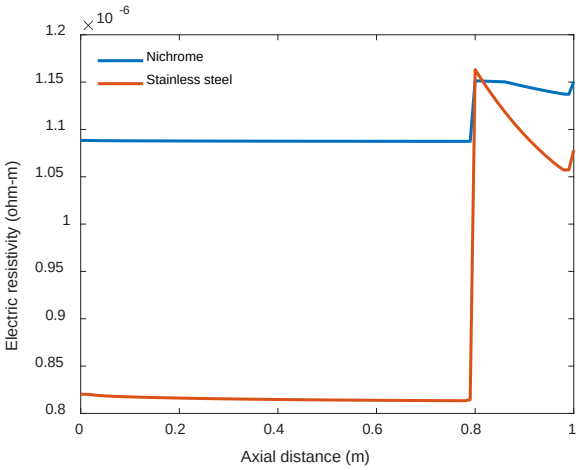

Figure 9. Electric resistivity distributions along the axial distance (semi-circular diameter of 2 mm)

3. Summary and conclusions

A printed circuit heat exchanger for the steam generator application is considered for the future PWR type SMRs. If an SMR produces superheated steam,

dryout will occur in the steam generator, and estimation of thermal fatigue induced by dryout in PCSG is not evaluated in detail previously. Hence, an experiment was planned to understand the phenomena. Experimental apparatus including the test section was designed with the unique concept of temperature measurement system. For further works, the experimental facility will be constructed to conduct the test and then compared to the analysis results.

ACKNOWLEDGEMENTS

This work was supported by the National Research Foundation of Korea(NRF) grant funded by the Korea government (Ministry of Science and ICT) (NRF-2020M2A8A4023945)

REFERENCES

[1] Shin, Chang Wook, and Hee Cheon No. "Experimental study for pressure drop and flow instability of two-phase flow in the PCHE-type steam generator for SMRs." *Nuclear Engineering and Design* 318 (2017): 109-118.
[2] Chiang, T., D. M. France, and T. R. Bump. "Calculation of tube degradation induced by dryout instability in sodium-heated steam generators." Nuclear Engineering and Design 41.2 (1977): 181-191.
[3] France, D. Mo, et al. "Characteristics of transition boiling in sodium-heated steam generator tubes." *Journal of Heat Transfer* 101.2 (1979): 270-275.
[4] Roko, K., K. Takitani, A. Yoshizaki, and M. Shiraha. "Dryout characteristics at low mass velocities in a vertical straight tube of a steam generator." In International Heat Transfer Conference Digital Library. Begel House Inc., 1978.
[5] Kwon, Jin Su, Sung Gil Shin, Jeong Ik Lee, and Sang Ji Kim. "Experimental printed circuit steam generator design for dryout induced thermal fatigue study." Transactions of the Korean Nuclear Society Autumn Meeting, Goyang, Korea, October 24-25, 2019
[6] Samra, S. S., and V. K. Dhir. "Study of thermal oscillations at the dryout front in half heated tubes." Journal of solar energy engineering 107.4 (1985): 343-351.
[7] Lomperski, S., C. Gerardi, and D. W. Pointer. "Distributed fiber optic temperature sensing for CFD code validation." In Proceedings of 15th International Topical Meeting on Nuclear Reactor Thermal Hydraulics (NURETH-15) Pisa, Italy, pp. 12-17. 2013.
[8] Gerardi, Craig, Nathan Bremer, Darius Lisowski, and Stephen Lomperski. "Distributed temperature sensor testing in liquid sodium." Nuclear Engineering and Design 312 (2017): 59-65.

Table I: Test section design results

Diameter (mm)	2	3	4
Material	Nichrome	Nichrome	Nichrome
Inlet temperature (°C)	90	100	100
Inlet quality	-0.018	0.33	0.45
Outlet temperature (°C)	110	110	110
Maximum wall temperature (°C)	538	493	481
Maximum heat flux (kW/m^2)	753	434	198
Preheater input / DC input (kW)	0 / 2.259	1 / 1.95	1 / 1.19
Voltage (V) / Current (A)	2.75 / 821	2.56 / 763	2 / 593
Mass flow rate (g/sec)	0.97	1.27	0.94
Mass flux (kg/m^2-sec)	620	360	150
Reynolds number	2411	2100	1167